



Bioreactor expansion reconfigures metabolism and extracellular vesicle biogenesis of human adipose-derived stem cells in vitro

Richard Jeske, Xingchi Chen, Shaoyang Ma, Eric Z. Zeng, Tristan Driscoll, Yan Li ^{*¹}

Department of Chemical and Biomedical Engineering, FAMU-FSU College of Engineering, Florida State University, USA



ARTICLE INFO

Keywords:

Human mesenchymal stem cells
Spinner bioreactor
Metabolism
Senescence
Extracellular vesicles

ABSTRACT

Human mesenchymal stem cells (hMSCs), including human adipose tissue-derived stem cells (hASCs), as well as the secreted extracellular vesicles (EVs), are promising therapeutics in treating inflammatory and neural degenerative diseases. However, prolonged expansion can lead to cellular senescence characterized by a gradual loss of self-renewal ability while altering secretome composition and EV generation. Additionally, hMSCs are highly sensitive to biophysical microenvironment in bioreactor systems utilized in scaling production. In this study, hASCs grown on Plastic Plus or Synthemax II microcarriers in a spinner flask bioreactor (SFB) system were compared to traditional 2D culture. The SFB microenvironment was found to increase the expression of genes associated with hASC stemness, nicotinamide adenine dinucleotide (NAD⁺) metabolism, glycolysis, and the pentose phosphate pathway as well as alter cytokine secretion (e.g., PGE2 and CXCL10). Elevated reactive oxidative species levels in hASCs of SFB culture were observed without increasing rates of cellular senescence. Expression levels of Sirtuins responsible for preventing cellular senescence through anti-oxidant and DNA repair mechanisms were also elevated in SFB cultures. In particular, the EV biogenesis genes were significantly upregulated (3–10 fold) and the EV production increased 40 % per cell in SFB cultures of hASCs. This study provides advanced understanding of hASC sensitivity to the bioreactor microenvironment for EV production and bio-manufacturing towards the applications in treating inflammatory and neural degenerative diseases.

1. Introduction

Human mesenchymal stem cells (hMSCs), including human adipose tissue-derived stem cells (hASCs), have been coveted in regenerative medicine for their multipotent differentiation abilities, secretome, and immunoprivilege [1,2]. Recent studies have demonstrated that their main therapeutic “mode of action” occurs through paracrine signaling as opposed to trans-differentiation or cell fusion [3–5]. While including cytokine/chemokine secretion, extracellular vesicles (EVs) and their smaller subset “exosomes” have gained significant distinction due to their natural or engineered ability to contain therapeutically relevant molecules (i.e., proteins, mRNAs, miRNA, drugs, etc.) when isolated from conditioned hMSC media [6,7]. The unique properties of hMSCs have led to unprecedented demand with the number of clinical trials for “mesenchymal stem cells” on clinicaltrials.gov nearly doubled since 2018. In anticipation of keeping up with clinical demand for hMSCs and their derived EVs, culture systems such as hollow-fiber, stirred-tank, and

vertical wheel bioreactors have been developed to maximize hMSC expansion [8–10]. However, little is known about the EV biogenesis of hMSCs, which are sensitive to biophysical microenvironment affecting their therapeutic properties, in bioreactor systems [11].

As with all non-immortalized somatic cells, the Hayflick limit applies to hMSCs through extended in vitro culture with the end result of replicative senescence [12–14]. With passaging, hMSCs have been observed to become progressively enlarged, undergo cytoskeleton rearrangement that changes spindle shape to irregular, alter surface marker expression, reduce differentiation capacity, and increase population doubling time until they are ultimately arrested in the cell cycle [12,15]. These alterations in phenotype elicited by extensive passaging have been shown to negatively affect preclinical and clinical trial outcomes [16,17]. For example, reduced behavioral and neurogenesis recovery after ischemic stroke have been observed in rats treated with intravenous administration of hMSCs at passage 6 compared to passage 2 [18]. Understanding the mechanisms modulating the breakdown in

* Correspondence to: 2525 Pottsdamer St, Tallahassee, FL 32310, USA.

E-mail addresses: rjj15@fsu.edu (R. Jeske), xc19a@fsu.edu (X. Chen), yanghohhot@gmail.com (S. Ma), zenge1995@gmail.com (E.Z. Zeng), tdriscoll2@eng.famu.edu (T. Driscoll), yli4@fsu.edu (Y. Li).

¹ ORCID: Yan Li: 0000-0002-5938-8519.

cellular homeostasis and progression towards replicative senescence in bioreactor culture is essential for the preservation of therapeutic properties of hMSCs for clinical use. However, the process of cellular senescence is complex and likely controlled by a number of factors such as progressive telomere shortening, DNA damage, oxidative stress, and accumulation of cyclin-dependent kinase inhibitor p16^{INK4a} [12,19,20].

Bioreactor culture may elevate reactive oxygen species (ROS), which are known to have integral roles in acting as cell signaling intermediates in differentiation, autophagy, immunomodulation, and senescence signaling pathways [21,22]. Our previous work has demonstrated accumulation of ROS in hMSCs after subjugation to shear stress (2–5 dyn/cm²) in a microcarrier-based spinner flask bioreactor (SFB) microenvironment [23]. ROS have been suggested as activators of autophagy in order to clear irreversibly oxidized biomolecules and relieve oxidative stress [24]. Furthermore, mitochondrial ROS have been shown to be required for immune suppressive indoleamine 2,3-dioxygenase (IDO) secretion induced with interferon (IFN)-γ [25]. Although the elucidation of exact mechanisms eliciting cellular senescence is ambiguous, ROS have been shown to contribute towards the senescent phenotype through direct damaging of the mitochondrial DNA contributing to oxidative phosphorylation (OXPHOS) dysfunction [26,27]. ROS supplemented through paracrine activity via neutrophils promoted premature senescence in fibroblasts by damaging telomeres [28]. However, how the ROS elevation affects hASC senescent behavior in the bioreactor culture is less known, although our previous study has reported the hASC senescent behavior during in vitro expansion in the 2D culture [29].

In this study, it is hypothesized that biophysical microenvironment encountered in a SFB could impact cellular metabolism of hASCs and alter senescence behaviors (e.g., Sirt expression, autophagy), compared to traditional 2D culture. It is further hypothesized that the microenvironment in the SFB culture could impact the secretion properties of hASCs such as cytokines and IDO secretion. In particular, the influence of suspension bioreactor culture on EV biogenesis and EV secretion of hASCs was investigated. The influence of bioreactor expansion of bone marrow hMSCs on the secreted EV production has been reported for the wave motion dynamic culture of hMSC aggregates and the Vertical-Wheel bioreactor culture of hMSCs on microcarriers in our previous studies [30,31]. This study provides additional insights into the hASC senescence behaviors and the secretome (containing cytokines and EVs) activities in scalable bioreactor culture systems for potential bio-manufacturing of hMSCs and the secreted EVs towards applications in treating neurological disorders, such as ischemic stroke and Alzheimer's disease.

2. Materials and methods

2.1. hASC culture

Frozen human adipose-derived MSCs (hASCs) at passage 1 were acquired from Tulane Center for Stem Cell Research and Regenerative Medicine. hASCs were isolated from the subcutaneous abdominal adipose tissue from de-identified healthy human donors. hASCs were characterized via colony-forming unit (CFU) assay and confirmed to possess tri-lineage differentiation potential (osteogenic, adipogenic and chondrogenic differentiation) in vitro [29,32]. Cells were received (1×10^6 cells/mL/vial) frozen in minimum essential medium-alpha (α-MEM) (Life Technologies, Carlsbad, CA) supplemented with 30 % fetal bovine serum (FBS), and 5 % dimethyl sulfoxide which were subsequently thawed and cultured in a manner described in our previous publications [25,33]. hASCs were seeded at a density of 2500 cells/cm² in 150 mm diameter Petri Dishes (Corning, Corning, NY) and cultured in a standard 5 % CO₂ incubator. Cells were cultured in α-MEM (containing 2 mM L-glutamine and 1 g/L glucose) supplemented with 10 % FBS (Atlanta Biologicals, Lawrenceville, GA) and 1 % Penicillin/Streptomycin (Life Technologies), defined as complete culture

medium (CCM). Media exchange was performed every 2–3 days. Upon reaching 80–90 % confluence, cells were harvested via incubation with 0.25 % trypsin/ ethylenediaminetetraacetic acid (EDTA) (Invitrogen, Grand Island, NY) for 5–7 min. Trypsin/EDTA solution was neutralized via addition of fresh serum-containing media. The collected solution was pelleted via centrifugation at 500 g for 5 min. Cell pellets were resuspended in 1 mL of fresh media and sampled with trypan blue for cell count and viability. hASCs were sub-cultured up to passage 6 before seeding in the SFBs.

2.2. Microcarrier-based suspension bioreactor culture

hASC expansion was achieved in a 125 mL Corning® Reusable Glass SFB (Corning, Corning, NY) inoculated at 3.6×10^4 cells/mL using 20 g/L Synthemax II microcarriers (360 cm²/gram, Corning, Corning, NY) or Plastic Plus microcarriers (360 cm²/gram, SoloHill) in CCM as the 2D controls. These two types of microcarriers were compared because they were used in our previous publications [23,30]. The SFB was autoclaved at 121 °C, 15 psi for 30 min prior to cell culture and pre-coated with sterile Sigmacote (Sigma) to prevent cell adhesion to the glass wall. The reactor was initially filled to 60 % working volume (60 mL) during the seeding phase and the impeller speed was set to 35 rpm. The intermittent agitation seeding method was used based on our previous studies [23,30]. The seeding phase consisted of 32 cycles each lasting 20 min. One cycle was complete after 4 min of agitation followed by 16 min of no agitation on a Wheaton Biostir® Stirrer system (DWK Life Sciences, Millville, NJ). On day 1, the media volume was raised to the working volume of 100 mL and the agitation was set at 50 or 80 rpm. 80 % media exchange was conducted every two days and samples were taken on day 1, 3, 5, and 7 to check growth kinetics and visually inspect the cells. Cell number was determined by Quant-iT™ PicoGreen kit (Invitrogen, Grand Island, NY). To visually inspect cell attachment, cells on microcarriers were stained with Hoechst 33342 (Thermofisher) to reveal cell nuclei and imaged under an Olympus IX70 microscope. After 7 days, cells were harvested for various assays.

For cell harvesting from microcarriers, cells and microcarriers were allowed to settle for 10 min. Conditioned media were then collected and stored at –80 °C. Bioreactors were filled to 50 % working volume of phosphate-buffered saline (PBS) and agitated at 25 rpm for 90 s, followed by 10 min settling. This washing process was repeated for three times. After the final washing, 50 % of PBS was replaced with Trypsin-EDTA (0.05 %) and incubated under 25 rpm agitation at 37 °C for 10 min. Bioreactor agitation was then increased to 80 rpm and incubated for another 5 min. An equal volume of media was added to quench Trypsin-EDTA and the microcarriers were allowed to settle. Supernatants containing cells were then collected and an additional rinse of PBS (25 % of working volume) was performed. Microcarriers were allowed to settle and supernatants were pooled together for centrifugation. Cells were pelleted and either stored at –80 °C or used immediately for characterizations.

2.3. DNA assay for cell number determination

Cell concentrations were determined with the Quant-iT™ PicoGreen kit (Invitrogen, Grand Island, NY), following the methods reported previously [25]. Briefly, cells were harvested, lysed over-night using proteinase K (VWR, Radnor, PA) at 50 °C, and stained with Picogreen (Molecular Probes, Eugene, OR). Fluorescence signals were read using a FluroCount (PerkinElmer, Boston, MA) and cellular DNA of samples was quantified using a standard curve. The fold expansion was calculated as the final cell density divided by the seeding cell density.

2.4. Colony forming unit-fibroblast (CFU-F) assay, β-gal activity, and enzyme-linked immunosorbent assay (ELISA)

For CFU-F assay, hASCs were harvested and re-plated at the density

of 15 cells/cm² on 60 cm² culture dish and grew for another 14 days in CCM. Cells were then stained with 20 % crystal violet solution in methanol (Sigma, St. Louis, MO) for 15 min at room temperature (RT) and gently washed with PBS three times. The number of individual colonies were counted manually. Cellular senescence was evaluated by SA- β -Gal activity assay kit (Sigma, St. Louis, MO) as described in manufacturer's instructions. The intensity was normalized to cell number.

Secreted Prostaglandin E2 (PGE2) and C-X-C motif chemokine ligand 10 (CXCL10) in cell culture supernatants were quantified using a PGE2 or CXCL10 Parameter Assay Kit (R&D Systems, Minneapolis, MN) according to manufacturer's instructions. Total secreted PGE2 or CXCL10 was determined by subtracting cytokine concentrations in culture media controls and normalized to cell number.

2.5. Western blot

Cell pellets of 1×10^6 cells or EV samples were lysed in radioimmunoprecipitation assay buffer (150 mM sodium chloride, 1.0 % Triton X-100, 0.5 % sodium deoxycholate, 0.1 % sodium dodecyl sulfate, 50 mM Tris, pH 8, all from Sigma) with addition of Halt Protease Inhibitor Cocktail (Fisher Scientific, Hampton, NH). Samples were incubated on ice for 20 min and centrifuged at 14,000 g for 20 min. The supernatants were collected and a Bradford assay (Bio-rad, Hercules, CA) was carried out to determine the protein concentration. Protein lysate concentration was normalized to the lowest sample concentration and then denatured at 100 °C in 2 x Laemmli Sample buffer for 5 min under reducing conditions (i.e., adding 2-Mercaptoethanol, Sigma). Proteins were separated by 12 % BIS-Tris-SDS gels and transferred onto a nitrocellulose membrane (Bio-rad, Hercules, CA). The membranes were blocked for 60 min in 5 % nonfat dry milk (w/v) in Tris-buffered saline (10 mM Tris-HCl, pH 7.5, and 150 mM NaCl) with 0.1 % Tween 20 (v/v) (TBST) and incubated overnight in the presence of the primary antibody (*Supplementary Table S1*) diluted in blocking buffer at 4 °C. Next, the membranes were washed three times with TBST and incubated with IR secondary antibodies (LI-COR, Lincoln, NE) at 1:5000 for three hours at room temperature. Membranes were washed three times in TBST and processed using the LI-COR Odyssey (LI-COR) system.

2.6. Measurement of IDO activity

IDO1 and IDO2 enzymatic activity, was assessed by measuring Kynurenine levels in cell culture supernatant. Cells attached to microcarriers were removed from the SFB and placed into ultra-low attachment 6-well plates. A 400 μ L of conditioned media, either stimulated by IFN- γ at 40 ng/mL, or left untreated for 24 h, was mixed with trichloroacetic acid (200 μ L, 30 % by weight; Sigma Aldrich, St. Louis, MO). Samples were centrifuged at 8000 g for 5 min. A 1:1 vol of 2 % p-dimethylaminobenzaldehyde in glacial acetic acid was added to the clarified supernatant and optical density at 490 nm was measured and normalized to cell number.

2.7. Flow cytometry for phenotyping

Cells were harvested from monolayer culture or microcarrier bioreactors by incubation with 0.25 % trypsin-EDTA solution for 5–7 min at 37 °C. Suspended hASCs were washed in PBS and fixed with 4 % paraformaldehyde (PFA) at room temperature for 15 min. Cells were then permeabilized in 0.2 % triton X-100 PBS for 10 min at room temperature. Nonspecific binding sites were blocked in PBS with 3 % bovine serum albumin, for 30 min at room temperature. Cells were washed with PBS and incubated with primary antibodies (*Supplementary Table S1*) at room temperature for two hours, followed by one hour incubation with the corresponding secondary antibody (Molecular Probe, Eugene, OR) at room temperature. Samples were washed in PBS and acquired (10,000 events) using BD FACSCanto II flow cytometer (Becton Dickinson) along with isotype control. The results were analyzed using FlowJo software.

The cellular debris were excluded based on the gating of the forward scatter (FSC) vs side scatter (SSC) plot.

2.8. ROS, autophagy, and cell cycle analysis

For ROS measurement, cell suspension was incubated with 25 μ M carboxy-H2DCFDA (Molecular Probe) at 37 °C for 30 min and total ROS was determined using flow cytometry. The samples not exposed to the fluorescent dye were used as the negative control. For mitochondrial ROS measurement, cell suspension was incubated with 5 μ M MitoSOX Red (Molecular Probe) at 37 °C for 10 min and analyzed using flow cytometry. ROS was also measured after three hours of exposure for SFB microenvironment. Treatment with a NADPH inhibitor apocynin (10 μ M, Sigma-Aldrich) [34] on the hASCs was also performed to evaluate mitochondria ROS levels.

For autophagy measurement, cell suspension was incubated with 20 μ M Cyto-ID Green (CYTO-ID® Autophagy detection kit, ENZ-51031, Enzo Life Sciences, Farmingdale, NY), a fluorescent dye that selectively labels accumulated autophagic vacuoles, at 37 °C for 30 min. The samples were analyzed by flow cytometry and the autophagy flux was calculated according to the manufacturer's instructions.

For cell cycle analysis, suspended cells were fixed with 70 % cold ethanol for 30 min at 4°C and then washed with PBS. RNase A (100 μ g/mL, VWR, Radnor, PA) was added to cell suspension and incubated at 37 °C for 15 min. The samples were incubated with 400 μ L 50 μ g/mL of propidium iodide (VWR) solution at RT in the dark for one hour. Cell cycle was then determined by flow cytometry.

2.9. Reverse transcription-polymerase chain reaction (RT-PCR)

Total RNA was isolated using TRIzol following vendor's instructions (Invitrogen). Reverse transcription was carried out using 2 μ g of total RNA, anchored oligo-dT primers (Operon) and Superscript III (Invitrogen). Primers for specific target genes were designed using the software Oligo Explorer 1.2 (Genelink) (*Supplementary Table S2*). β -actin was used for normalization as the housekeeping gene after comparison with GAPDH. RT-PCR reactions were performed using SYBR Green PCR Master Mix on an ABI7500 instrument (Applied Biosystems). The amplification reactions were performed as follows: 2 min at 50 °C; 10 min at 95 °C; and 40 cycles of 95 °C for 15 s; 55 °C for 30 s; and 68 °C for 30 s. The quality and primer specificity were verified. Fold variations in gene expressions were quantified using the $\Delta\Delta Ct$ method: $2^{-\Delta(\Delta Ct_{Treatment} - Ct_{Control})}$, in comparison to the 2D culture.

2.10. Extracellular vesicle isolation

For EV isolation experiments, culture media were replaced by EV-depleted media (the growth medium with the FBS depleted of EVs by ultracentrifugation) on day 5 and collected on day 7. Conditioned media were sequentially spun (500 g for 5 min, 2000 g for 10 min, 10,000 g for 30 min) to remove cell debris, apoptotic body, large vesicles, etc. Polyethylene glycol (PEG)- 6000 was added to the supernatant to a final end ratio of 8 % PEG and 0.5 M NaCl and stored for 24 h at 4 °C as previously demonstrated [35] in order to enrich EVs. The solution was spun at 3000 g for one hour and supernatant discarded. Remaining pellet was suspended in 1 mL PBS and ultracentrifuged at 120,000 g using the SW-28 swing-bucket rotor in an Optima XL-100 K ultracentrifuge (k factor-15, Beckman Coulter Inc.) for 70 min at 4 °C. The EV pellet was then suspended in 200 μ L PBS and disrupted using a benchtop shaker at 1500 rpm for 5 min. EVs were diluted to 10^8 - 10^9 particles per mL in PBS for nanoparticle tracking analysis.

2.11. Nanoparticle tracking analysis (NTA)

Nanoparticle tracking analysis (NTA) was performed on the isolated EV samples in triplicate to determine size distribution and EV

concentration. NTA was performed on a Nanosight LM10-HS instrument (NTA 3.4 Build 3.4.003, Malvern Instruments, Malvern, UK) configured with a blue (488 nm) laser and sCMOS camera [36]. For each replicate, three videos of 60 s were acquired with camera shutter speed fixed at 30.00 ms. To ensure accurate and consistent detection of small particles, camera level was set to 13, and detection threshold was maintained at three. The laser chamber was cleaned thoroughly with particle-free water between each sample reading. The collected videos were analyzed using NTA3.0 software to obtain the mode and mean size distribution, as well as the concentration of particles per mL of solution. Compared to the mean size, the mode size is usually a more accurate

representation because the vesicle aggregates may affect the value of mean size.

2.12. Statistical analysis

Unless otherwise noted, all experiments were performed at least three times with triplicate biological samples ($n = 3$). The data from the representative experiments were reported. Experimental results were expressed as means \pm standard deviation (SD) of the samples. Data were analyzed in Graphpad Prism software. Statistical comparisons were performed by one-way ANOVA and Tukey's post hoc test for multiple

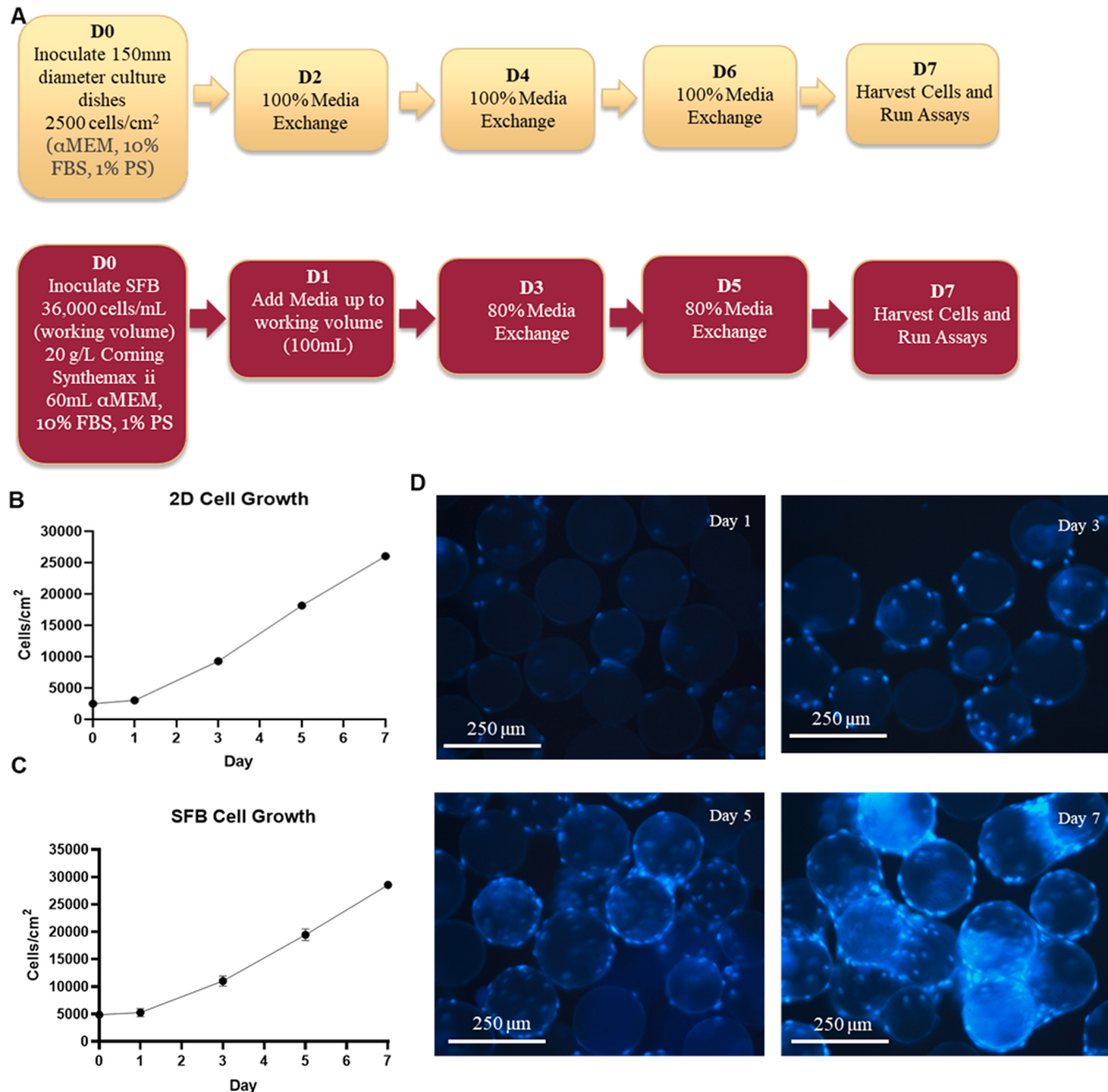


Fig. 1. hMSC expansion in microcarrier-based spinner bioreactors. (A) Schematic representation of experimental procedure. (B) 2D cell counts show near linear growth over 7-day culture period. (C) Bioreactor cell growth mimics 2D growth curve. (D) Hoescht nuclear stain shows cell growth on microcarriers and cell/microcarrier aggregation as cell density increases. Scale bar: 250 μ m. Synthemax II microcarriers: 360 cm^2/gram , 20 g/L. For 100 mL (0.1 L), 2 g was used, then total surface area was 720 cm^2 . The bioreactor was inoculated with 3.6×10^4 cells/mL, 100 mL for 3.6×10^6 cells, $3.6 \times 10^6 \text{ cells}/720 \text{ cm}^2 = 5000 \text{ cells}/\text{cm}^2$. The seeding efficiency was 50–70 %. For 50 % seeding efficiency, the seeding density was 2500–3500 cells/ cm^2 . 2D culture seeding density was 2500 cells/ cm^2 .

comparisons, and significance was accepted at $p < 0.05$.

3. Results

3.1. Expansion and characterization of microcarrier-based bioreactor expansion of hASCs

As illustrated in Fig. 1A, hASC expansion was performed in a 125 mL Corning® Reusable Glass Spinner Flask Bioreactor in parallel to traditional 2D culture (morphology shown in Supplementary Fig. S1) using hASCs from different donors (Supplementary Fig. S2). Briefly, the SFB was inoculated with 3.6×10^4 cells/mL using 20 g/L Synthemax II microcarriers (equivalent to 5.0×10^3 cells/cm²), which were selected after the comparison with Plastic Plus microcarriers (Supplementary Fig. S3). The seeding efficiency on microcarriers was about 50–70 %, which was about $2.5\text{--}3.5 \times 10^3$ cells/cm². In parallel, hASCs were seeded into 150 mm plastic culture dishes at 2.5×10^3 cells/cm² as 2D control. Media were exchanged every two days and the cells were harvested on day 7. Both 2D and SFB culture kinetics followed a near linear expansion with 2D group reaching roughly 2.6×10^4 cells/cm² (10.4-fold expansion) on day 7 (Fig. 1B) and the SFB group reaching over 2×10^5 cells/mL (6.1-fold) (Fig. 1C). Nuclear staining showed even cell distribution among microcarriers with the majority of microcarriers containing one or more hASCs (Fig. 1D). After day 5, the aggregation of cells and multiple microcarriers was observed as cell densities reached

greater than 1.5×10^5 cells/mL.

Next, the properties commonly known in hMSCs during cellular senescence were investigated [29,37]. Compared to the 2D culture, no statistically significant difference ($p > 0.05$) was observed in SFB-expanded hASCs for CFU ability (Fig. 2A), the indication for stem cell content, and β -gal activity, a known biomarker for cellular senescence (Fig. 2B) [38]. mRNA expression of the stemness markers *Nanog*, *Sox2*, and *Oct4* was significantly upregulated ($p < 0.05$) in the SFB culture (~4–6 fold) (Fig. 2C). However, the mRNA expression of tumor suppression genes *P15*, *P21*, *P53*, and *P16* was also upregulated in the SFB culture (~1.5–9 fold) compared to the 2D culture (Fig. 2D). Cell cycle analysis showed that the SFB culture had a higher proportion (17 % vs. 6 %) of G2 cells and fewer G1 cells (77 % vs. 91 %) compared to the 2D culture, indicating more active cell cycle progression for hASCs adhered on microcarriers (Supplementary Fig. S4). These results demonstrated that the SFB culture altered senescence behaviors and stemness of hASCs compared to the 2D culture.

3.2. ROS accumulation, autophagy, and metabolic status in bioreactor-expanded hASCs

Then, the indicators related to the mitochondrial function and metabolic status of the hASCs were evaluated. The total ROS was increased in the SFB culture compared to the 2D group (Fig. 3A and Supplementary Fig. S5). Similarly, mitochondrial ROS were also

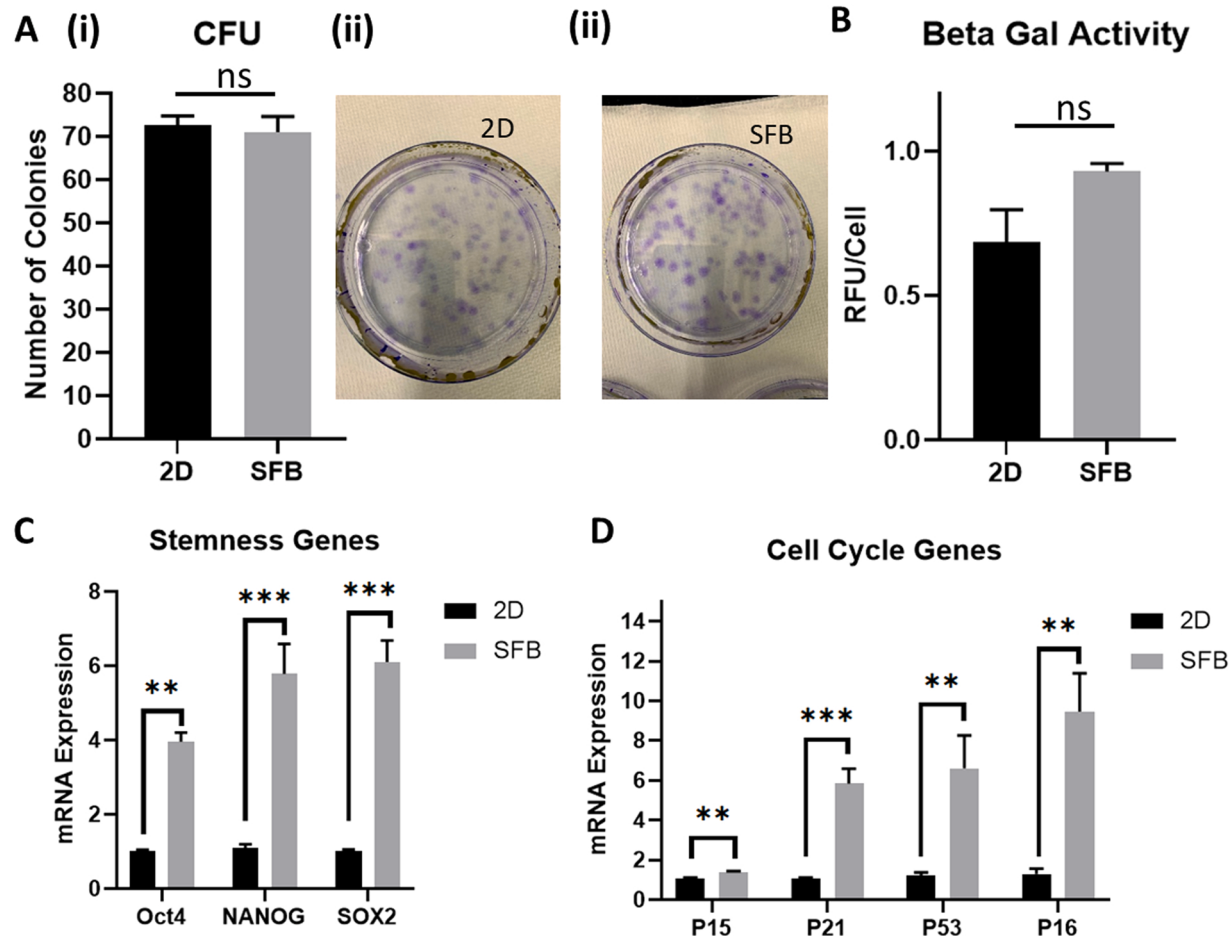


Fig. 2. Characterizations of bioreactor-expanded hMSCs-cell cycle and stemness. (A) CFU ability was not impacted by SFB culture. (i) Number of colonies for the 2D and SFB conditions; Representative images for the CFU numbers for the (ii) 2D and (iii) SFB conditions. 60 cm² culture dishes were used for this assay. (B) Senescence-associated β -gal marker did not significantly increase in SFB culture. (C) mRNA levels of genes (determined by RT-PCR) controlling stem cell multipotency were upregulated in SFB culture. (D) mRNA levels of genes (determined by RT-PCR) controlling cell cycle and senescence were upregulated in SFB culture. Data expressed as means \pm standard deviation (SD). N = 3. * indicates $p < 0.05$; ** indicates $p < 0.01$; *** indicates $p < 0.001$; ns: not significant.

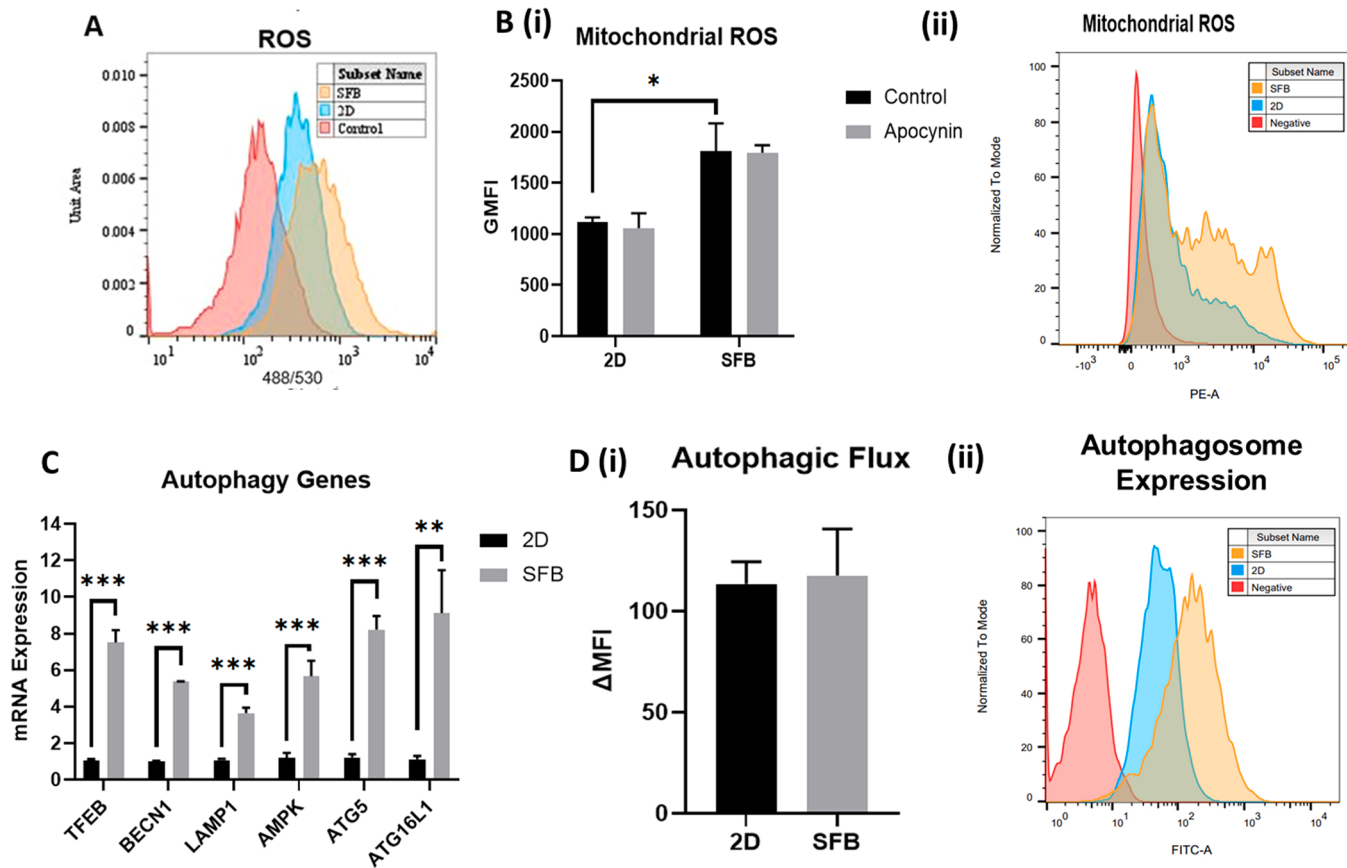


Fig. 3. Characterizations of bioreactor-expanded hMSCs-ROS, Sirt1/3, and autophagy. (A) Total ROS was increased in SFB culture compared to 2D culture. (B) Mitochondrial ROS was upregulated in SFB. (i) The average mean fluorescence intensity determined by flow cytometry. (ii) The representative flow cytometry histogram. Red: negative control; Blue: 2D condition; Orange: SFB culture. Apocynin treatment had no effect on mitochondrial ROS levels. (C) RT-PCR demonstrated that mRNA levels of genes regulating autophagy were upregulated in SFB culture compared to 2D culture. (D) Autophagic flux remained at similar levels before and after culture in the SFB. However, total levels of autophagosomes were increased after subjected to SFB microenvironment. (i) The average mean fluorescence intensity change determined by flow cytometry. (ii) The representative flow cytometry histogram. Red: negative control; Blue: 2D condition; Orange: SFB culture. Data expressed as means \pm standard deviation (SD). N = 3. * indicates $p < 0.05$; ** indicates $p < 0.01$, *** indicates $p < 0.001$. (For interpretation of the references to color in this figure legend, the reader is referred to the web version of this article.)

upregulated in the SFB culture (Fig. 3B). Treatment with a NADPH inhibitor apocynin had no impact on mitochondrial ROS levels. mRNA levels of genes responsible for regulating autophagy (*TFEB*, *BECN1*, *LAMP1*, and *AMPK*), including the genes linked to the secretion of exosomes (*ATG5* and *ATG16L1*), were found to be upregulated (4–8 fold) in the SFB group potentially as an added layer of defense against accumulated ROS (Fig. 3C). Interestingly, despite the increased total ROS accumulation in the SFB-cultured cells, autophagic flux remained at the comparable level between the two groups (Fig. 3D). However, there was greater accumulation of autophagosomes in the SFB-cultured hASCs.

To evaluate the influence of shear stress levels on the metabolic gene expression, the SFB was run at both 50 rpm (average shear stress is ~ 3 dyn/cm 2) and 80 rpm (average shear stress is ~ 6 dyn/cm 2). mRNA levels of genes responsible for regulating the pentose phosphate pathway (PPP), *G6PD* and *6PGD*, for the SFB culture at 50 rpm did not show statistically differences compared to the 2D group, but the expression increased at 80 rpm (~ 1.5 fold) (Fig. 4A). However, *TALDO1*, a mediator linked to nucleic acid and lipid biosynthesis, and *TKTL1*, a key mediator between glycolysis and the PPP, showed upregulation (1.5–2 fold) in the SFB cultures at both 50 rpm and 80 rpm. RT-PCR also revealed that *PDK1* and *PKM2* had similar expression between the 2D and SFB groups while *HK2* showed significant upregulation (2–6 fold, $p < 0.05$) in the SFB group (Fig. 4B). For *LDHA*, the gene that encodes for the lactate dehydrogenase A subunit, the expression was

decreased (about 50 %) in the SFB group.

For NAD $^+$ consuming enzyme *CD73* and the rate-limiting enzyme in the NAD $^+$ salvage pathway, *NAMPT*, the expression showed upregulation (~ 1.5 –2.5 fold) in the SFB group compared to the 2D group (Fig. 4C). The *CD38* expression was also significantly increased (3–6 fold, $p < 0.05$) in the SFB culture. As previously mentioned, there is growing evidence that Sirtuins are essential in delaying cellular senescence and extending lifespan through the prevention of telomere shortening and the promotion of DNA damage repair [37,39,40]. mRNA levels of *Sirt-1* (1.5–3 fold) and *Sirt-3* (~ 1.2 fold) were elevated in the SFB culture compared to the 2D culture (Fig. 4C). The increased *Sirt-1* (Fig. 4D) and *Sirt-3* (Fig. 4E) protein levels were also observed in the SFB-cultured hASCs measured by flow cytometry, which was further confirmed using Western blot assay (Fig. 4F). These results demonstrated that the SFB culture altered the metabolic gene expression of hASCs and elevated the ROS and autophagy in the cells.

3.3. The inflammatory responses of bioreactor-expanded hASCs under IFN- γ licensing

Our previous study showed that extended in vitro culture of hASCs in 2D culture significantly shifted cytokine and chemokine secretion towards pro-inflammatory phenotype [29]. Here the inflammatory responses of hASCs expanded in dynamic SFB culture under IFN- γ licensing were evaluated. IDO activity via relative quantities of

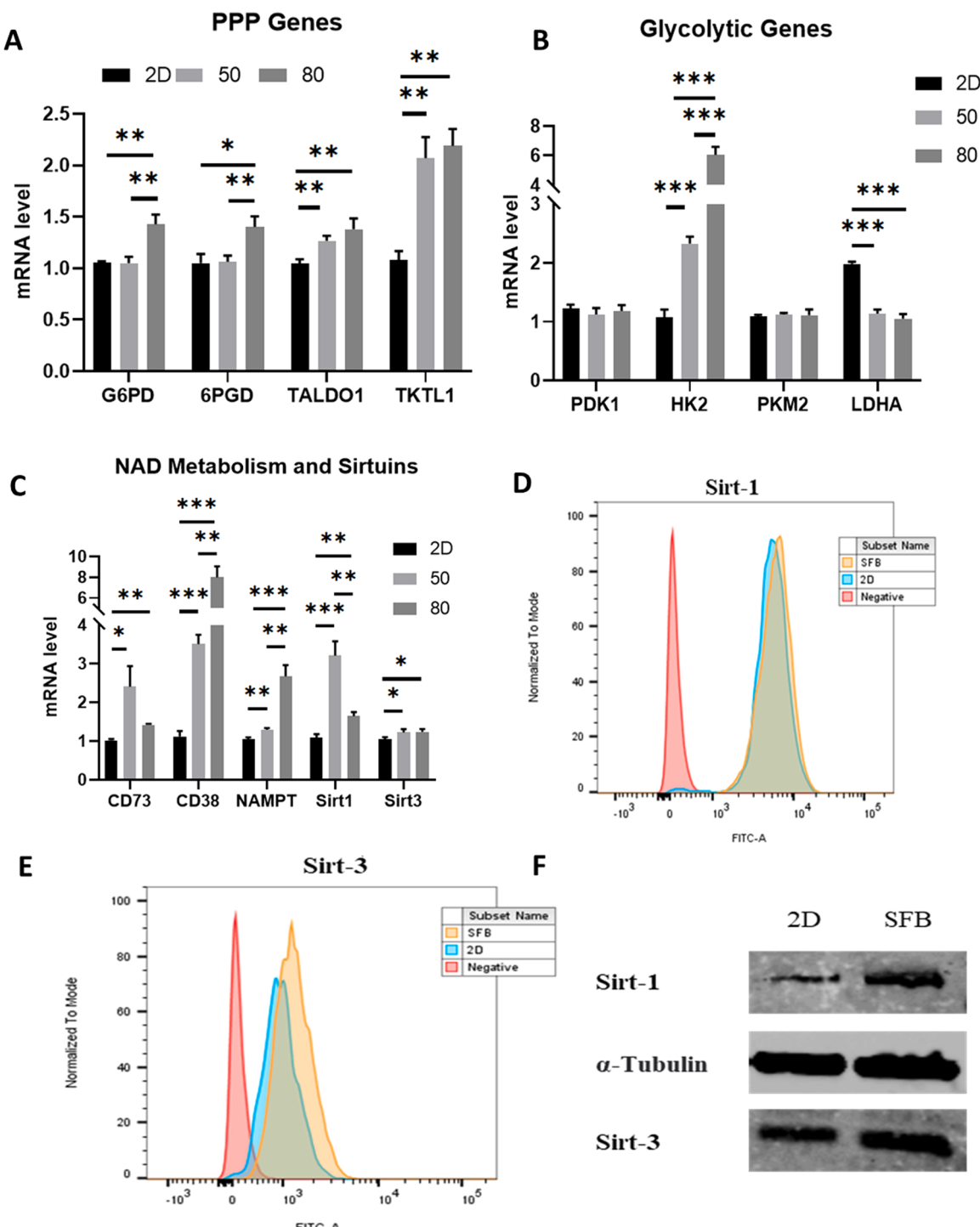


Fig. 4. Expression of genes associated with metabolism pathways in bioreactor-expanded hMSCs. mRNA levels in 2D culture compared to SFB culture at 50 rpm or 80 rpm for (A) PPP genes; (B) Glycolysis genes, (C) NAD Metabolism and Sirtuins, determined by RT-PCR. mRNA levels of Sirt-1 and Sirt-3 are elevated in SFB culture. Flow cytometry histograms for (D) Sirt1 and (E) Sirt3 expression. (F) Western blot bands for Sirt1 and Sirt3 expression. Protein expression of Sirt-1 remains constant regardless of culture conditions while Sirt-3 was upregulated in SFB culture. Data expressed as means \pm standard deviation (SD). N = 3. * indicates $p < 0.05$; ** indicates $p < 0.01$, *** indicates $p < 0.001$.

kynurenone, the metabolite of tryptophan catabolized by IDO necessary for immune cell suppression [41], was increased before and post IFN- γ licensing for the cells from the SFB group compared to the 2D group (Fig. 5A). After IFN- γ treatment, hMSCs were “licensed” to exert the immunomodulatory effect through the activation of IDO enzyme. Therefore, the fold-change in hMSCs represents the potentials to modulate local inflammatory environments. The increased secretion

before and after IFN- γ licensing in the SFB-cultured hASCs was also observed for the pro-inflammatory cytokine CXCL10 (Fig. 5B). The agitation at 80 rpm further increased CXCL10 secretion compared to the 50 rpm group. However, the ratio of post/before licensing was significantly lower for the SFB culture than the 2D group ($p < 0.05$). For anti-inflammatory cytokine PGE2, a decrease in the SFB group at 80 rpm before IFN- γ treatment was observed, and there was no significant

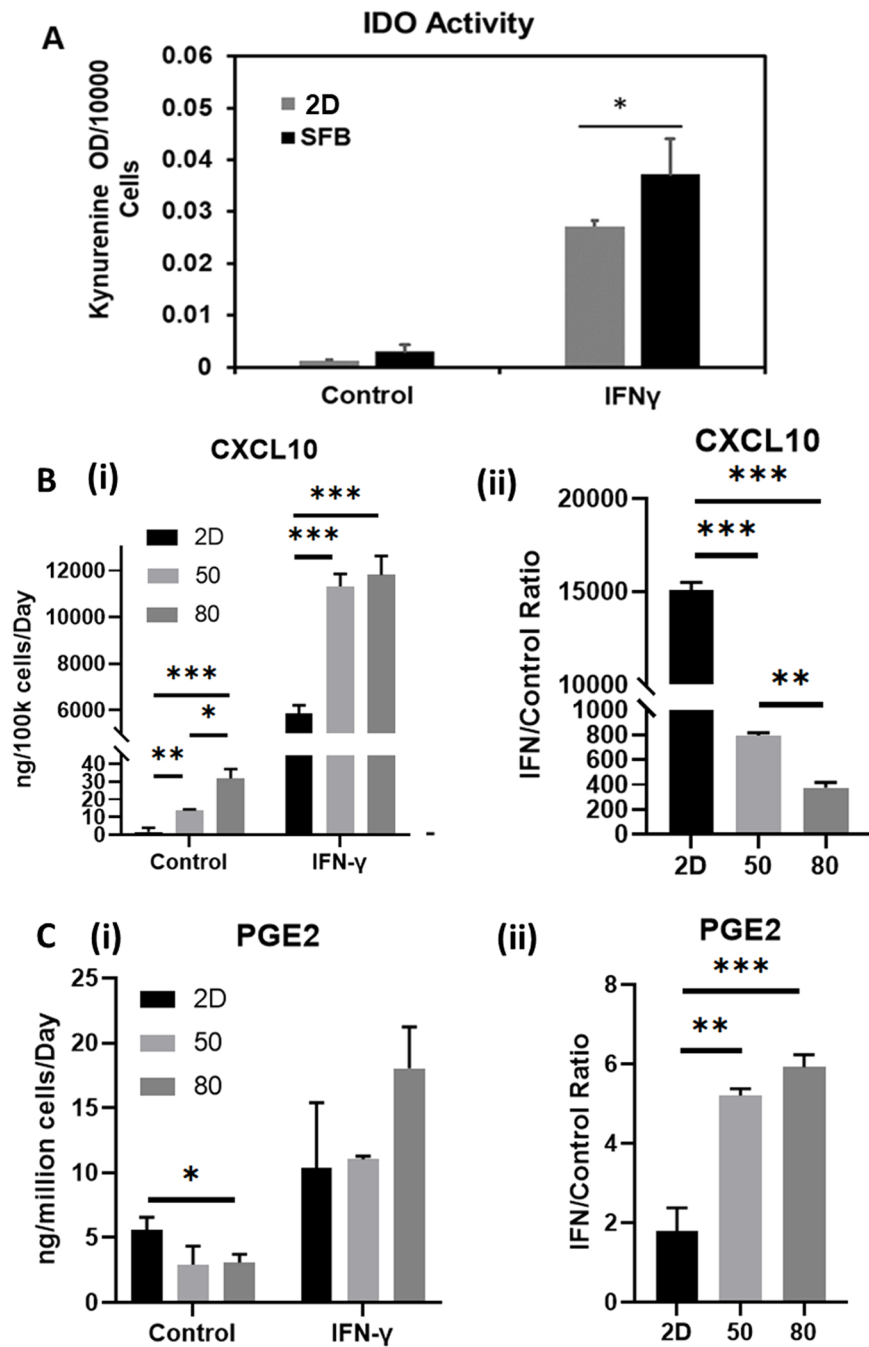


Fig. 5. IDO activity and cytokine secretion for bioreactor-expanded hMSCs. (A) Kynurenine concentrations were increased in SFB culture both before and after licensing with IFN- γ . (B) CXCL10 secretion by hMSCs was increased in SFB culture (50 and 80 rpm) compared to 2D culture. (i) CXCL10 amount determined by ELISA normalized to cell number and time; (ii) The ratio of secretion under IFN- γ stimulation to control. (C) PGE2 secretion was decreased in the SFB group before treatment with IFN- γ . Post treatment levels remained at similar levels for the three conditions. (i) PGE2 amount determined by ELISA normalized to cell number and time; (ii) The ratio of secretion under IFN- γ stimulation to control. Data expressed as means \pm standard deviation (SD). N = 3. * indicates p < 0.05; ** indicates p < 0.01, *** indicates p < 0.001.

difference ($p > 0.05$) after the IFN- γ treatment for the SFB group compared to the 2D group (Fig. 5C). However, the ratio of post/prior licensing was significantly higher ($p < 0.05$) for the SFB culture than the 2D culture. These results demonstrated that the SFB culture altered the inflammatory responses of hASCs under IFN- γ licensing.

3.4. Extracellular vesicle biogenesis of hASCs in bioreactors

To date, the EV biogenesis of hASCs in the bioreactor microenvironment has been less understood. Here, the mRNA levels for genes critical to the endosomal sorting complex required for transport (ESCRT)-dependent and independent EV biogenesis were measured. The ESCRT-dependent genes (*STAM1*, *ALIX*, *TSG101*, and *HRS*) were all upregulated by 3–5 fold in the SFB culture compared to the 2D group (Fig. 6A). For ESCRT-independent genes and GTPases measured, the

expression was upregulated by 3.5–4.0 fold (*SMPD2*, *SMPD3*, *Rab7a*, *Rab31*, and *Rab27a*) for the SFB group compared to the 2D group with *Rab27b* showing 10-fold higher expression (Fig. 6B). NTA measurements revealed similar EV size distributions between the 2D and SFB groups with distribution peaks around 60 nm, 130 nm, 160 nm, and 290 nm (Fig. 6C). Neither group showed statistically significant differences ($p > 0.05$) in EV mean or mode size distributions (Fig. 6D). NTA measurements also showed a 40 % increase in EV secretion per cell base in the SFB group compared to the 2D group. The SFB group almost doubled the media productivity (EVs per mL of media used) compared to the 2D group. Western blot analysis revealed that the isolated EVs had the positive expression of exosomal markers syntenin-1 and CD81 and no expression for the negative exosomal marker calnexin (Fig. 6E). These results demonstrated that the SFB culture promoted the EV biogenesis and EV secretion.

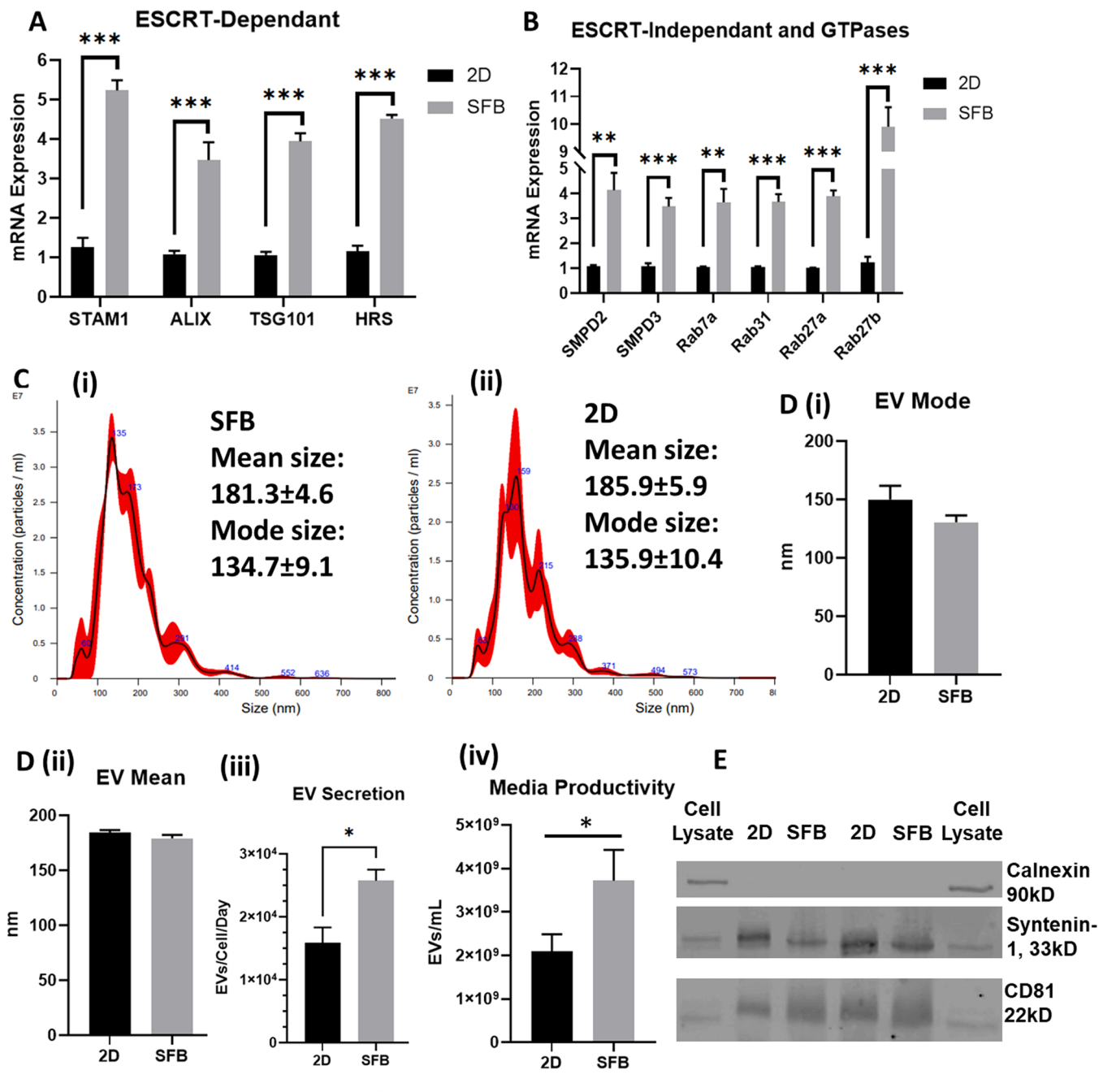


Fig. 6. EV biogenesis of hASCs expanded in the spinner flask bioreactor. mRNA levels of genes for EV biogenesis: (A) ESCRT-dependent; (B) ESCRT-independant and GTPases, determined by RT-PCR. (C) NTA analysis for the EV size distribution. (i) SFB condition; (ii) 2D condition. (D) EV characterizations (i) mode size; (ii) mean size; (iii) the number of the secreted EVs normalized to cell number; (iv) the EV yields normalized as medium productivity. (E) Western blot of exosomal markers for the isolated EVs: Calnexin (a negative EV marker), Syntenin-1 and CD81 (the positive EV markers). Data expressed as means \pm standard deviation (SD). N = 3. * indicates $p < 0.05$; ** indicates $p < 0.01$, *** indicates $p < 0.001$.

4. Discussion

In this study, hASCs were expanded in SFB achieving cell density over 2×10^5 cells/mL (a clinically relevant dose is 2×10^6 hMSCs/kg) and the impacts of biophysical microenvironment in SFB on ROS accumulation, senescence, and EV production were assessed and compared to traditional 2D culture. hMSC expansion has been shown to be affected by hMSC tissue source, passage number, microcarrier type, bioreactor system, and donor variations [30,42]. The SFB microenvironment led to an accumulation of total and mitochondrial ROS consistent with our previous study using different microcarriers [23]. The mitochondrial free radical theory of aging or “Oxidative Stress Theory” is one proposed

hypothesis modulating the breakdown of cellular homeostasis, and ultimately, cellular senescence [43–45]. Generation of excessive high energy ROS or a loss of antioxidant defenses has been thought to lead to irreversible damage to lipids, proteins, and nucleic acids. Accumulation of DNA damage, damaged telomeres, and redox-sensitive proteins may promote the senescent phenotype with growth cycle arrest and a phenotype shift with senescence-associated pro-inflammatory secretome, thus contributing to age-related pathology [46,47]. However, the hMSC senescence behavior and EV biogenesis in the dynamic bioreactor systems have not been well investigated.

Despite elevated ROS levels in SFB, CFU ability and the known hallmark of replicative senescence, β -gal activity, were not statistically

altered in SFB culture compared to 2D control. However, senescence and loss of stem cell function is a process that occurs gradually through extended culture periods and may not be easily discernable through one passage in bioreactors [29,37,48]. Serial hMSC passage in bioreactors may need to use a bead-to-bead transfer procedure [49], which needs to be tested and optimized in our culture system in future studies. The tumor suppression genes *P15*, *P16*, *P21*, and *P53* were investigated in this study for their potential as biomarkers for “pre-senescence”, which describes a point where cells lose their proliferative growth but do not yet outwardly present classical characteristics of senescence [50]. The SFB culture showed upregulation of these four genes compared to the 2D control and continued elevation could have significant impacts on cell cycle arrest [51]. For example, p21 and p53 activation can lead to arrest at the G1/S or G2/M checkpoints and actually inhibit apoptosis, exacerbating the senescent cascade [52].

Interestingly, the stemness genes (*Oct4*, *Nanog*, and *Sox2*) were also upregulated in SFB culture compared to 2D group, indicating that the cells were primitive and the senescence behavior of hASCs in SFB is different from 2D culture. Traditionally, oxidative stress and loss of multipotency is associated with senescence in stem cells [53]. However, ROS are known to play key roles as cell signaling intermediates in lineage-specific differentiation in the Wnt, Hedgehog, and FOXO signaling cascades, and elevated levels have been suggested to inhibit osteogenesis and promote adipogenesis [21]. The tri-lineage potential after SFB culture is well documented in the literature [54–56], hence not evaluated in this study. For example, spinner flask culture has been shown with significantly lower intracellular Ca^{+} and osteocalcin concentrations after osteogenic differentiation of hMSCs compared to static culture [57]. Our previous study also showed that dynamic culture of hMSCs promoted the adipogenic and osteogenic differentiation compared to the 2D culture [31].

Shear stress has been shown to increase mitochondrial ROS production primarily through NADPH and c-Jun N-terminal Kinase (JNK)-1/JNK-2 phosphorylation [58]. Following treatment with apocynin, a NADPH oxidase inhibitor, hASCs in SFB in this study were found to possess mitochondrial ROS levels similar to the control, suggesting that the hASC ROS response to shear stress is different from endothelial cells and not through NADPH. hMSCs were reported to respond to intermittent shear stress by the Ras-dependent extracellular signal-regulated kinase (ERK)1/2 activation and the upregulation of mechanosensitive genes (e.g., *PTGS2*, *IER3*, *FGF2*, and *VEGFA*) as well as additional nitric oxide generation, suggesting additional ROS generation sources in bioreactor culture [59]. However, mitochondrial respiration is generally the main source of ROS generation in mitochondrial complex I and III [21]. Regardless of source, interplay between ROS and autophagy has been reported as one of the main cellular defenses to combat excessive ROS accumulation [24,60–62]. In this study, the genes responsible for the regulation of autophagic processes (i.e., *TFEB*, *BECN1*, *LAMP1*, *AMPK*, *ATG5* and *ATG16L1*) were upregulated in the SFB group compared to the 2D control. However, autophagic flux levels were comparable for the two conditions. Despite the unchanged total flux, total autophagosome levels were increased in the SFB-cultured hASCs. The increased accumulation may have cytotoxic effects and lead to cell death when autophagosome-lysosomal fusion is blocked [63].

In order to assess the impact of bioreactor microenvironment on hASC metabolism, the SFB was run at both 50 and 80 rpm. The shear stress profiles (1–9 dyn/cm² using COMSOL) for the SFB have been reported in our previous work [23]. While PPP genes *TALDO1* and *TKTL1* were upregulated at the 50 rpm condition compared to 2D control, the 80 rpm condition further increased their expression, suggesting that the PPP activation commits more glucose 6-phosphate to the PPP away from glycolysis [64]. The 80 rpm condition also upregulated *G6PD* and *6PGD*, which is essential for NADPH replenishment [65]. *HK2* catalyzes phosphorylates glucose and is the only gene upregulated in the SFB culture, suggesting that more glucose may be committed to glycolysis and the PPP [66]. However, changes in other glycolytic genes were not observed

with the exception of *LDHA*, suggesting that the PPP maybe utilize more glucose 6-phosphate. The influence of shear stress levels (25 rpm, 40 rpm, and 64 rpm) on EV biogenesis has been evaluated in our previous study [30]. Our results show that the conditions of all the three stirring speeds promoted the EV secretion compared to the 2D control, but there were no significant differences ($p > 0.05$) among 25 rpm, 40 rpm, and 64 rpm conditions.

Furthermore, SFB upregulated main NAD⁺ consuming enzymes (*CD73*, *CD38*, *Sirt-1*, and *Sirt-3*) that may contribute to the depletion of the NAD⁺ pool and rely upon the Sirtuins in preventing senescence and mediating oxidative stress [67]. The Sirt-1 and Sirt-3 protein expression could be beneficial to the longevity of the cells [68,69]. Interestingly, Sirt-3 is located in the mitochondria and may be upregulated as an antioxidant defense of the hASCs. Sirt-3 directly deacetylates manganese superoxide dismutase (enhancing the ability to scavenge ROS) as well as IDH2 in the tricarboxylic acid cycle, which produces NADPH and ultimately generate new anti-oxidant molecules [69]. Additionally, the SFB culture increased IDO activity before and after IFN- γ treatment and promoted the secretion of anti-inflammatory cytokine under IFN- γ stimulation. ROS have been known to affect hMSC secretome, IDO secretion, as well as a number of cell signaling pathways related to cytokine secretion. ROS regulation of IDO activity may be a possible mechanism for this observed increase [25]. Together, the bioreactor microenvironments alter the hASC senescence behavior, cellular metabolism, and cytokine secretion.

Recently, it has been suggested paracrine action through EVs or exosomes is the main mechanistic mode of action for hMSCs in wound healing and tissue regeneration [70,71]. However, hMSC secretome and therapeutic potential is heavily influenced by microenvironmental parameters, including oxygen tension, inflammatory stimulus, aggregation, etc. [72]. Therefore, the impacts of SFB microenvironment on EV secretion was assessed in this study (Supplementary Fig. S6). The expression for both ESCRT-dependent and independent EV biogenesis genes was upregulated in the SFB culture compared to the 2D culture, which led to 40 % increase in the secreted EV quantity per cell base. There is a growing body of literature suggesting that autophagy and EV biogenesis may be intimately linked and share much of the similar cellular machinery [73–75]. Indeed, higher levels of genes responsible for modulation of autophagy were observed in SFB culture (i.e., *TFEB*, *BECN1*, *LAMP1*, and *AMPK*) as well as *ATG5* and *ATG16L1*, which have been proven critical to EV biogenesis in preventing the acidification of the lysosome and lysosomal exocytosis [75,76]. While this did not correspond to greater overall levels of autophagic flux in SFB-cultured hMSCs, greater levels of autophagosomes via flow cytometry were observed. Further investigations into autophagosome accumulation and EV secretion as well as EV cargo analysis could yield insights into the mechanisms controlling the promoted EV biogenesis in bioreactors. Our previous study has shown that the PBS VerticalWheel bioreactor promoted EV biogenesis and the secreted EV cargo showed increased miRNA levels and expression of therapeutic proteins in protein cargo [30]. The influence of different bioreactor configurations and the hydrodynamics on the EV cargo profiles remains to be explored.

For potential clinical applications of using hMSC-secreted EVs (a clinical relevant dose is $\sim 4 \times 10^{10}$), the scale up of the bioreactor system is required. Our previous study has shown the scale up from 0.1 L bioreactors to 0.5 L bioreactors [30]. However, with scale up, the oxygen transfer become more challenging, and the inclusion of medium perfusion or gas sparging may become necessary.

5. Conclusion

In this study, expansion of hASCs in the SFB reaching cell density over 2×10^5 cells/mL was demonstrated. The SFB microenvironment led to accumulation of total and mitochondrial ROS, which had implications on cell fate, autophagy, and secretome while not significantly impacting cellular senescence. Furthermore, SFB culture promoted EV

biogenesis and EV/exosome secretion, with a 40 % increase of EV number per cell base and a two-fold increase in the yield of EV number per mL spent media compared to 2D culture. Together, these findings demonstrate the impacts of bioreactor microenvironments on hASC metabolism and the EV biogenesis. The implications of this study enable the scale-up processes for biomanufacturing of hASCs and the secreted EVs for future clinical applications such as in Alzheimer's disease, ischemic stroke, and multiple sclerosis.

Funding

This study is supported by National Science Foundation (NSF 1743426)-CBET: Advanced Biomanufacturing program. Research reported in this publication was also partially supported by the National Institutes of Health (USA) under Award Number R01NS125016. The content is solely the responsibility of the authors and does not necessarily represent the official views of the National Institutes of Health.

Author contribution

RJ performed the majority of the work and wrote the initial draft of the manuscript. XC, SM, and EZ helped with the sample preparation and characterization. TD participated in discussion and revised the manuscript. YL perceived the experiments, revised and finalized the manuscript.

CRediT authorship contribution statement

Conceptualization: X.Y. and Y.L.; Data curation: R.J., X.C.; Formal analysis: R.J., X.C., S.M., E.Z., T.D., Y.L.; Funding acquisition: Y.L.; Investigation: R.J., X.C., S.M., E.Z., T.D., Y.L.; Methodology: R.J., X.C., S.M., E.Z.; Project administration: Y.L.; Resources: Y.L.; Supervision: Y.L.; Validation: R.J.; Visualization: R.J., X.C.; Writing – original draft: R.J. and Y.L.; Writing – review & editing: T.D. and Y.L.

Declaration of Competing Interest

The authors declare the following financial interests/personal relationships which may be considered as potential competing interests: Yan Li reports was provided by National Institutes of Health. Richard Jeske reports was provided by National Science Foundation.

Data availability

Data will be made available on request.

Acknowledgement

The authors would like to thank Dr. Brian K. Washburn at Florida state university (FSU) Department of Biological Sciences for their help with RT-PCR analysis, and the support from Flow Cytometry Core Facility.

Appendix A. Supporting information

Supplementary data associated with this article can be found in the online version at [doi:10.1016/j.bej.2022.108711](https://doi.org/10.1016/j.bej.2022.108711).

References

- [1] M.F. Pittenger, D.E. Discher, B.M. Péault, D.G. Phinney, J.M. Hare, A.I. Caplan, Mesenchymal stem cell perspective: cell biology to clinical progress, *npj Regen. Med.* 4 (2019) 22.
- [2] W. Faiella, R. Atoui, Immunotolerant properties of mesenchymal stem cells: updated review, *Stem Cells Int.* 2016 (2016).
- [3] X. Liang, Y. Ding, Y. Zhang, H.F. Tse, Q. Lian, Paracrine mechanisms of mesenchymal stem cell-based therapy: current status and perspectives, *Cell Transpl.* 23 (2014) 1045–1059.
- [4] I. Linero, O. Chaparro, Paracrine effect of mesenchymal stem cells derived from human adipose tissue in bone regeneration, *PLoS One* 9 (2014).
- [5] S.H. Ranganath, O. Levy, M.S. Inamdar, J.M. Karp, Harnessing the mesenchymal stem cell secretome for the treatment of cardiovascular disease, *Cell Stem Cell* 10 (2012) 244–258.
- [6] Y. Liang, L. Duan, J. Lu, J. Xia, Engineering exosomes for targeted drug delivery, *Theranostics* 11 (2021) 3183–3195.
- [7] S. Nikfarjam, J. Rezaie, N.M. Zolbanin, R. Jafari, Mesenchymal stem cell derived-exosomes: a modern approach in translational medicine, *J. Transl. Med.* 18 (2020) 449.
- [8] J. Gobin, G. Muradia, J. Mehic, C. Westwood, L. Couvrette, A. Stalker, S. Bigelow, C.C. Luebert, F.S.-D. Bissonnette, M.J.W. Johnston, S. Sauvé, R.Y. Tam, L. Wang, M. Rosu-Myles, J.R. Lavoie, Hollow-fiber bioreactor production of extracellular vesicles from human bone marrow mesenchymal stromal cells yields nanovesicles that mirrors the immuno-modulatory antigenic signature of the producer cell, *Stem Cell Res. Ther.* 12 (2021) 127.
- [9] T. Lawson, D.E. Kehoe, A.C. Schnitzler, P.J. Rapiejko, K.A. Der, K. Philbrick, S. Punredy, S. Rigby, R. Smith, Q. Feng, J.R. Murrell, M.S. Rook, Process development for expansion of human mesenchymal stromal cells in a 50L single-use stirred tank bioreactor, *Biochem. Eng. J.* 120 (2017) 49–62.
- [10] D. de Sousa Pinto, C. Bandeiras, M. de Almeida Fuzeta, C.A.V. Rodrigues, S. Jung, Y. Hashimura, R.J. Tseng, W. Milligan, B. Lee, F.C. Ferreira, C. Lobato da Silva, J. M.S. Cabral, Scalable manufacturing of human mesenchymal stromal cells in the vertical-wheel bioreactor system: an experimental and economic approach, *Biotechnol. J.* 14 (2019), e1800716.
- [11] A.-C. Tsai, R. Jeske, X. Chen, X. Yuan, Y. Li, Influence of microenvironment on mesenchymal stem cell therapeutic potency: from planar culture to microcarriers, *Front. Bioeng. Biotechnol.* 8 (2020) 640.
- [12] W. Wagner, P. Horn, M. Castoldi, A. Diehlmann, S. Bork, R. Saffrich, V. Benes, J. Blake, S. Pfister, V. Eckstein, A.D. Ho, Replicative senescence of mesenchymal stem cells: a continuous and organized process, *PLoS One* 3 (2008).
- [13] J. Liu, Y. Ding, Z. Liu, X. Liang, Senescence in mesenchymal stem cells: functional alterations, molecular mechanisms, and rejuvenation strategies, *Front. Cell Dev. Biol.* 8 (2020) 258.
- [14] A. Schellenberg, Q. Lin, H. Schüler, C.M. Koch, S. Joussen, B. Denecke, G. Walenda, N. Pallua, C.V. Suschek, M. Zenke, W. Wagner, Replicative senescence of mesenchymal stem cells causes DNA-methylation changes which correlate with repressive histone marks, *Aging* 3 (2011) 873–888.
- [15] X. Zhou, Y. Hong, H. Zhang, X. Li, Mesenchymal stem cell senescence and rejuvenation: current status and challenges, *Front. Cell Dev. Biol.* 8 (2020) 364.
- [16] L. von Bahr, L. Sundberg B Fau - Lönnies, B. Lönnies L Fau - Sander, H. Sander B Fau - Karbach, H. Karbach H Fau - Hägglund, P. Hägglund H Fau - Ljungman, B. Ljungman P Fau - Gustafsson, H. Gustafsson B Fau - Karlsson, K. Karlsson H Fau - Le Blanc, O. Le Blanc K Fau - Ringdén, O. Ringdén, Long-term Complications, Immunologic Effects, and Role of Passage for Outcome in Mesenchymal Stromal Cell Therapy.
- [17] P.R. Crisostomo, M. Wang, G.M. Wairiuko, E.D. Morrell, A.M. Terrell, P. Seshadri, U.H. Nam, D.R. Meldrum, High Passage Number of Stem Cells Adversely Affects Stem Cell Activation and Myocardial Protection, *Shock* 26 (2006).
- [18] W.Y. Li, Y.J. Choi, P.H. Lee, K. Huh, Y.M. Kang, H.S. Kim, Y.H. Ahn, G. Lee, O. Y. Bang, Mesenchymal stem cells for ischemic stroke: changes in effects after ex vivo culturing, *Cell Transplant.* 17 (2008) 1045–1059.
- [19] J. Liu, Y. Ding, Z. Liu, X. Liang, Senescence in mesenchymal stem cells: functional alterations, molecular mechanisms, and rejuvenation strategies, *Front. Cell Dev. Biol.* 8 (2020).
- [20] Y. Li, Q. Wu, Y. Wang, L. Li, H. Bu, J. Bao, Senescence of mesenchymal stem cells (Review), *Int. J. Mol. Med.* 39 (2017) 775–782.
- [21] F. Atashi, A. Modarressi, M.S. Pepper, The role of reactive oxygen species in mesenchymal stem cell adipogenic and osteogenic differentiation: a review, *Stem Cells Dev.* 24 (2015) 1150–1163.
- [22] S. Sart, L. Song, Y. Li, Controlling redox status for stem cell survival, expansion and differentiation, *Oxid. Med. Cell. Longev.* 2015 (2015), 105135.
- [23] R. Jeske, S. Lewis, A.C. Tsai, K. Sanders, C. Liu, X. Yuan, Y. Li, Agitation in a microcarrier-based spinner bioreactor modulates homeostasis of human mesenchymal stem cells, *Biochem. Eng. J.* 168 (2021), 107947.
- [24] G. Filomeni, D. De Zio, F. Cecconi, Oxidative stress and autophagy: the clash between damage and metabolic needs, *Cell Death Differ.* 22 (2015) 377–388.
- [25] Y. Liu, X. Yuan, N. Munoz, T.M. Logan, T. Ma, Commitment to aerobic glycolysis sustains immunosuppression of human mesenchymal stem cells, *Stem Cells Transl. Med.* 8 (2019) 93–106.
- [26] P. Davalli, T. Mitic, A. Caporali, A. Lauriola, D. D'Arca, ROS, cell senescence, and novel molecular mechanisms in aging and age-related diseases, *Oxid. Med. Cell. Longev.* 2016 (2016).
- [27] N. Nissanka, C.T. Moraes, Mitochondrial DNA damage and reactive oxygen species in neurodegenerative disease, *FEBS Lett.* 592 (2018) 728–742.
- [28] A. Lagnado, J. Leslie, M.-H. Ruchaud-Sparagano, S. Victorelli, P. Hirsova, M. Ogrodnik, A.L. Collins, M.G. Vizioli, L. Habiballa, G. Saretzki, S.A. Evans, H. Salmonowicz, A. Hruba, D. Geh, K.D. Pavelko, D. Dolan, H.L. Reeves, S. Grellscheid, C.H. Wilson, S. Pandanaboyana, M. Doolittle, T. von Zglinicki, F. Oakley, S. Gallage, C.D. Wilson, J. Birch, B. Carroll, J. Chapman, M. Heikenwalder, N. Neretti, S. Khosla, C.A. Masuda, T. Tchkonka, J.L. Kirkland, D. Jurk, D.A. Mann, J.F. Passos, Neutrophils induce paracrine telomere dysfunction and senescence in ROS-dependent manner, *EMBO J.* 40 (2021), e106048.

- [29] R. Jeske, X. Yuan, Q. Fu, B. Bunnell, T.M. Logan, Y. Li, In vitro culture expansion shifts the immune phenotype of human adipose-derived mesenchymal stem cells, *Front Immunol.* 12 (2021), 621744.
- [30] R. Jeske, C. Liu, L. Duke, M.L. Canonico Castro, L. Muok, P. Arthur, M. Singh, L. Sung, L. Sun, Y. Li, Upscaling human mesenchymal stem cell production in a novel vertical wheel bioreactor enhances extracellular vesicle secretion and cargo profile, *Bioact. Mater.* (2022).
- [31] X. Yuan, L. Sun, R. Jeske, D. Nkosi, S. York, Y. Liu, S.C. Grant, D.G.J. Meckes, Y. Li, Engineering extracellular vesicles by three-dimensional dynamic culture of human mesenchymal stem cells, *J. Extracell. Vesicles* 11 (2022), e12235.
- [32] B.M. Bijnowski, Q. Fu, X. Yuan, J. Irianto, Y. Li, S.C. Grant, T. Ma, Aggregation-induced integrated stress response rejuvenates stemness of culture-expanded human mesenchymal stem cells, *Biotechnol. Bioeng.* 117 (2020) 3136–3149.
- [33] L. Song, X. Yuan, Z. Jones, K. Griffin, Y. Zhou, T. Ma, Y. Li, Assembly of human stem cell-derived cortical spheroids and vascular spheroids to model 3-D brain-like tissues, *Sci. Rep.* 9 (2019) 5977.
- [34] M.S. Petronio, M.L. Zeraik, L.M. Fonseca, V.F. Ximenes, Apocynin: chemical and biophysical properties of a NADPH oxidase inhibitor, *Molecules* 18 (2013) 2821–2839.
- [35] M.A. Rider, S.N. Hurwitz, D.G. Meckes, ExtraPEG: a polyethylene glycol-based method for enrichment of extracellular vesicles, *Sci. Rep.* 6 (2016) 23978.
- [36] M.A. Rider, S.N. Hurwitz, D.G. Meckes Jr., ExtraPEG: a polyethylene glycol-based method for enrichment of extracellular vesicles, *Sci. Rep.* 6 (2016) 23978.
- [37] X. Yuan, Y. Liu, B. Bijnowski, A.C. Tsai, Q. Fu, T.M. Logan, T. Ma, Y. Li, NAD+/NADH redox alterations reconfigure metabolism and rejuvenate senescent human mesenchymal stem cells in vitro, *Commun. Biol.* 3 (2020) 774.
- [38] F. Debacq-Chainiaux, J.D. Eruaslimsky, J. Campisi, O. Toussaint, Protocols to detect senescence-associated beta-galactosidase (SA- β gal) activity, a biomarker of senescent cells in culture and in vivo, *Nat. Protoc.* 4 (2009) 1798–1806.
- [39] S.I. Imai, L. Guarente, It takes two to tango: NAD(+) and sirtuins in aging/longevity control, *NPJ Aging Mech. Dis.* 2 (2016) 16017.
- [40] S. Imai, J. Yoshino, The importance of NAMPT/NAD/SIRT1 in the systemic regulation of metabolism and ageing, *Diabetes Obes. Metab.* 15 (Suppl 3) (2013) 26–33.
- [41] W. Ling, J. Zhang, Z. Yuan, G. Ren, L. Zhang, X. Chen, A.B. Rabson, A.I. Roberts, Y. Wang, Y. Shi, Mesenchymal stem cells use IDO to regulate immunity in tumor microenvironment, *Cancer Res.* 74 (2014) 1576–1587.
- [42] A.C. Tsai, R. Jeske, X. Chen, X. Yuan, Y. Li, Influence of microenvironment on mesenchymal stem cell therapeutic potency: from planar culture to microcarriers, *Front. Bieng. Biotechnol.* 8 (2020) 640.
- [43] A. Chandrasekaran, M.D.P.S. Idechik, J.A. Melendez, Redox control of senescence and age-related disease, *Redox Biol.* 11 (2017) 91–102.
- [44] R. Buffenstein, Y.H. Edrey, T. Yang, J. Mele, The oxidative stress theory of aging: embattled or invincible? Insights from non-traditional model organisms, *Age* 30 (2008) 99–109.
- [45] K.C. Kregel, H.J. Zhang, An integrated view of oxidative stress in aging: basic mechanisms, functional effects, and pathological considerations, *Am. J. Physiol. Regul. Integr. Comp. Physiol.* 292 (2007) R18–R36.
- [46] I. Liguori, G. Russo, F. Curcio, G. Bulli, L. Aran, D. Della-Morte, G. Gargiulo, G. Testa, F. Cacciatore, D. Bonaduce, P. Abete, Oxidative stress, aging, and diseases, *Clin. Interv. Aging* 13 (2018) 757–772.
- [47] B. Schöttker, H. Brenner, E.H.J.M. Jansen, J. Gardiner, A. Peasey, R. Kubínová, A. Pajak, R. Topor-Madry, A. Tamasiunas, K.-U. Saum, B. Hollecze, H. Pikhart, M. Bobak, Evidence for the free radical/oxidative stress theory of ageing from the CHANCES consortium: a meta-analysis of individual participant data, *BMC Med.* 13 (2015) 300.
- [48] J. Liu, Y. Ding, Z. Liu, X. Liang, Senescence in mesenchymal stem cells: functional alterations, molecular mechanisms, and rejuvenation strategies, *Front. Cell Dev. Biol.* 8 (2020) 258.
- [49] Q.A. Rafiq, S. Ruck, M.P. Hanga, T.R.J. Heathman, K. Coopman, A.W. Nienow, D. J. Williams, C.J. Hewitt, Qualitative and quantitative demonstration of bead-to-bead transfer with bone marrow-derived human mesenchymal stem cells on microcarriers: utilising the phenomenon to improve culture performance, *Biochem. Eng. J.* 135 (2018) 11–21.
- [50] S.R. Schwarze, Y. Shi, V.X. Fu, P.A. Watson, D.F. Jarrard, Role of cyclin-dependent kinase inhibitors in the growth arrest at senescence in human prostate epithelial and uroepithelial cells, *Oncogene* 20 (2001) 8184–8192.
- [51] H. Rayess, M.B. Wang, E.S. Srivatsan, Cellular senescence and tumor suppressor gene p16, *Int. J. Cancer* 130 (2012) 1715–1725.
- [52] M. Mijit, V. Caracciolo, A. Melillo, F. Amicarelli, A. Giordano, Role of p53 in the regulation of cellular senescence, *Biomolecules* 10 (2020) 420.
- [53] V. Turinetto, E. Vitale, C. Giachino, Senescence in human mesenchymal stem cells: functional changes and implications in stem cell-based therapy, *Int. J. Mol. Sci.* 17 (2016) 1164.
- [54] P.A. Tozetti, S.R. Caruso, A. Mizukami, T.R. Fernandes, F.B. da Silva, F. Traina, D. T. Covas, M.D. Orellana, K. Swiech, Expansion strategies for human mesenchymal stromal cells culture under xeno-free conditions, *Biotechnol. Prog.* 33 (2017) 1358–1367.
- [55] M.F.Q. Sousa, M.M. Silva, D. Giroux, Y. Hashimura, R. Wesselschmidt, B. Lee, A. Roldão, M.J.T. Carrondo, P.M. Alves, M. Serra, Production of oncolytic adenovirus and human mesenchymal stem cells in a single-use, Vertical-Wheel bioreactor system: impact of bioreactor design on performance of microcarrier-based cell culture processes, *Biotechnol. Prog.* 31 (2015) 1600–1612.
- [56] D. Egger, I. Schwedhelm, J. Hansmann, C. Kasper, Hypoxic three-dimensional scaffold-free aggregate cultivation of mesenchymal stem cells in a stirred tank reactor, *Bioengineering* 4 (2017) 47.
- [57] H.-H. Tsai, K.-C. Yang, M.-H. Wu, J.-C. Chen, C.-L. Tseng, The effects of different dynamic culture systems on cell proliferation and osteogenic differentiation in human mesenchymal stem cells, *Int. J. Mol. Sci.* 20 (2019) 4024.
- [58] W. Takabe, N. Jen, L. Ai, R. Hamilton, S. Wang, K. Holmes, F. Dharbandi, B. Khalsa, S. Bressler, M.L. Barr, R. Li, T.K. Hsiao, Oscillatory shear stress induces mitochondrial superoxide production: implication of NADPH oxidase and c-Jun NH2-terminal kinase signaling, *Antioxid. Redox Signal.* 15 (2011) 1379–1388.
- [59] P. Becquart, M. Cruel, T. Hoc, L. Sudre, K. Pernelle, R. Bizios, D. Logear-Avramoglou, H. Petite, M. Bensidhoum, Human mesenchymal stem cell responses to hydrostatic pressure and shear stress, *Eur. Cell Mater.* 31 (2016) 160–173.
- [60] M.B. Azad, Y. Chen, S.B. Gibson, Regulation of autophagy by reactive oxygen species (ROS): implications for cancer progression and treatment, *Antioxid. Redox Signal.* 11 (2009) 777–790.
- [61] C. Fang, L. Gu, D. Smerin, S. Mao, X. Xiong, The interrelation between reactive oxygen species and autophagy in neurological disorders, *Oxid. Med. Cell. Longev.* 2017 (2017), 8495160.
- [62] S. Kongara, V. Karanta, The interplay between autophagy and ROS in tumorigenesis, *Front. Oncol.* 2 (2012).
- [63] R.W. Button, S.L. Roberts, T.L. Willis, C.O. Hanemann, S. Luo, Accumulation of autophagosomes confers cytotoxicity, *J. Biol. Chem.* 292 (2017) 13599–13614.
- [64] E.S. Cho, Y.H. Cha, H.S. Kim, N.H. Kim, J.I. Yook, The pentose phosphate pathway as a potential target for cancer therapy, *Biomol. Ther.* 26 (2018) 29–38.
- [65] R.C. Stanton, Glucose-6-phosphate dehydrogenase, NADPH, and cell survival, *IUBMB Life* 64 (2012) 362–369.
- [66] D.J. Roberts, S. Miyamoto, Hexokinase II integrates energy metabolism and cellular protection: aktng on mitochondria and TORCing to autophagy, *Cell Death Differ.* 22 (2015) 248–257.
- [67] S.H. Lee, J.H. Lee, H.Y. Lee, K.J. Min, Sirtuin signaling in cellular senescence and aging, *BMB Rep.* 52 (2019) 24–34.
- [68] C. Chen, M. Zhou, Y. Ge, X. Wang, SIRT1 and aging related signaling pathways, *Mech. Ageing Dev.* 187 (2020), 111215.
- [69] B. Kincaid, E. Bossy-Wetzel, Forever young: SIRT3 a shield against mitochondrial meltdown, aging, and neurodegeneration, *Front. Aging Neurosci.* 5 (2013).
- [70] P. Ahangar, S.J. Mills, A.J. Cowin, Mesenchymal stem cell secretome as an emerging cell-free alternative for improving wound repair, *Int. J. Mol. Sci.* 21 (2020) 7038.
- [71] B.F. Hettich, M. Ben-Yehuda Greenwald, S. Werner, J.-C. Leroux, Exosomes for wound healing: purification optimization and identification of bioactive components, *Adv. Sci.* 7 (2020), 2002596.
- [72] S. Wangler, A. Kamali, C. Wapp, K. Wuertz-Kozak, S. Häckel, C. Fortes, L. M. Benneker, L. Haglund, R.G. Richards, M. Alini, M. Peroglio, S. Grad, Uncovering the secretome of mesenchymal stromal cells exposed to healthy, traumatic, and degenerative intervertebral discs: a proteomic analysis, *Stem Cell Res. Ther.* 12 (2021) 11.
- [73] G. Pedrioli, P. Paganetti, Hijacking endocytosis and autophagy in extracellular vesicle communication: where the inside meets the outside, *Front. Cell Dev. Biol.* 8 (2021).
- [74] J.M. Gudbergsson, K.B. Johnsen, Exosomes and autophagy: rekindling the vesicular waste hypothesis, *J. Cell Commun. Signal.* 13 (2019) 443–450.
- [75] L. Salimi, A. Akbari, N. Jabbari, B. Mojarrad, A. Vahhab, S. Szafert, S.A. Kalashani, H. Soraya, M. Nawaz, J. Rezaie, Synergies in exosomes and autophagy pathways for cellular homeostasis and metastasis of tumor cells, *Cell Biosci.* 10 (2020) 64.
- [76] N. Gammoh, The multifaceted functions of ATG16L1 in autophagy and related processes, *J. Cell Sci.* 133 (2020).